Available online at www.sciencedirect.com

SciVerse ScienceDirect

Procedia CIRP 8 (2013) 194 – 199

www.elsevier.com/locate/procedia

14th CIRP Conference on Modeling of Machining Operations (CIRP CMMO)

Modeling and Experimental Investigation of Edge Hone and Flank Contact Effects in Metal Cutting

Ceren Çelebi[a], E. Özlü[b], Erhan Budak[c]*

[a]*Manufacturing Research Lab., Sabanci University, Istanbul 34956, Turkey*
[b]*Maxima Manufacturing R&D Inc., Kocaeli, Turkey*
* Corresponding author. Tel.: +90-216-483-95-50.*E-mail address*: ebudak@sabanciuniv.edu.

Abstract

In this study, a process model for orthogonal cutting is developed in order to determine the effect of the hone radius and flank contact on cutting forces. A thermo-mechanical model at primary shear zone with sticking and sliding contact zones on the rake face is used for cutting forces and these contact zones are implemented in the third deformation zone. The model predictions are verified by experiments using carbide inserts with various hone radii at different speeds and feeds.

Selection and peer-review under responsibility of The International Scientific Committee of the "14th CIRP Conference on Modeling of Machining Operations" in the person of the Conference Chair Prof. Luca Settineri

Keywords: Machining process modeling; orthogonal cutting; hone radius, flank contact

1. Introduction

Being one of the most important parameters in cutting tools, hone radius has important effects on cutting mechanics, surface quality, tool life and overall production efficiency. Due to the hone radius a third deformation zone exists, which contributes in formation of edge cutting forces. Although numerous models have been proposed for primary and secondary shear zones, there are only few models which cover the third deformation zone and edge forces.

In an earlier study, Albrecht [1] introduced hone radiused tools and presented a force diagram including ploughing forces. Later, Endres [2] developed an analytical model which includes the effect of hone radius explicitly by studying deformation under the hone edge. In a later study Kountanya and Endres [3] investigated cutting process with cameras which has high magnification properties in order to verify the aforementioned model. It is found out that the basic model is not sufficient in order to represent the deformation in front of the hone radius and a model which includes the deformation precisely is needed.

Slip-line field modelling has been widely used in modelling of the third deformation zone [4-5]. These models focus on the deformation under tool, but there is not a unified modelling approach.

Experimental studies are also carried out in order to understand the cutting process with honed tools [6-11]. As a common conclusion cutting forces increases as the hone radius increases. Moreover temperature at the tool tip increases with the increasing hone radius.

Finite element analysis has also been used in order to observe the effect on the stress-strain conditions, as well as temperature on the third deformation zone [12-15]. Although FEM analysis can give more insight about the cutting process, the solution times are generally high. Also, the true friction between the tool and workpiece material cannot be identified in the simulation programs or other models. Studies are continuing in order to identify the third deformation zone using FEM.

In this paper, a process model representing the third deformation zone is proposed with the implementation of sticking and sliding contact zones on the hone. Cutting forces, pressure distributions at the flank and rake faces can be calculated by the proposed model. The proposed model is verified with the experiments conducted on AISI 1050 steel using tools with different hone radii.

Selection and peer-review under responsibility of The International Scientific Committee of the "14th CIRP Conference on Modeling of Machining Operations" in the person of the Conference Chair Prof. Luca Settineri
doi:10.1016/j.procir.2013.06.088

2. Modeling of Orthogonal Cutting

In this section the proposed model is presented. The basic orthogonal cutting model with a radiused tool is shown in Fig. 1 where (AB) represents primary and secondary shear zones and (AC) represents third deformation zone. Point A is defined as stagnation point, where the material just above this point creates chip while the lower sections form the flank contact. Primary and secondary shear zones are effective above stagnation point, whereas below this point represented by third deformation zone.

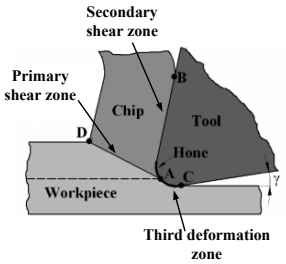

Fig. 1: Deformation zones in orthogonal cutting.

2.1. Primary and secondary shear zones

In the proposed approach thermomechanical material model is used for the primary shear zone. Material behaviour is represented with the Johnson-Cook constitutive model, and the minimum energy approach is used for the shear angle prediction [16]. As for the secondary shear zone the rake contact which is above the stagnation point is divided into three regions (Fig. 2: Regions R1, R2, and R3) for mathematical simplicity. Then, the dual-zone model developed by Ozlu et al. [17] is applied. Briefly, in the model the rake face is divided into two friction zones where the regions close to the tool-tip is represented by sticking friction and the rest is by sliding friction model.

2.2. Third deformation zone

The contact area below the stagnation point is referred to as the third deformation zone (Fig. 2a: Regions R4, R5, and R6) and is responsible for the ploughing and the flank contact due to elastic recovery. The third deformation zone is divided into three regions again for mathematical simplicity.

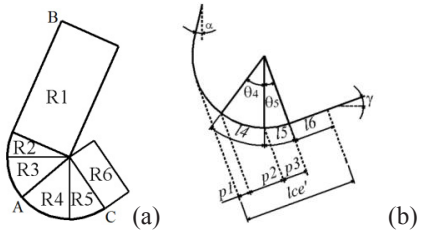

Fig. 2: (a) Hone-radiused cutting tool model with the divided regions; (b) Contact length and length projections on the clearance face.

Normal pressure and shear stress distributions

In this study the contact at the hone and flank surfaces are divided into sticking and sliding friction regions. Expected normal pressure and shear stress distributions along the sticking and sliding zones can be seen in Fig. 3 and are defined as follows:

$$P(\chi) = P_0\left(1 - \frac{\chi}{l_{ce}}\right)^{\zeta} \qquad 0 \le \chi \le l_{ce} \tag{1}$$

$$\tau = \tau_1 \qquad 0 \le \chi \le l_{pe} \tag{2}$$

$$\tau = \mu P \qquad l_{pe} \le \chi \le l_{ce}$$

where, P is the normal pressure distribution, P_0 is the normal pressure constant, χ is the distance from the stagnation point, l_{ce} is the contact length on the flank surface (Fig. 4), ζ is the stress distribution exponent, $\boldsymbol{\tau}_1$ is the shear stress at the exit of the primary shear zone, μ is the sliding friction coefficient between tool and workpiece and l_{pe} is the sticking contact length.

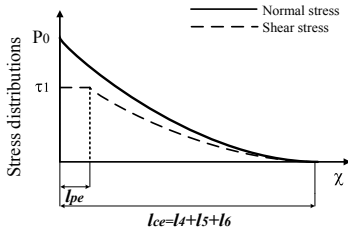

Fig. 3: The normal pressure and the shear stress distributions in the third deformation zone.

Contact Length in the Third Deformation Zone

Although the ultimate aim is to estimate the contact length analytically, in this preliminary study the measured contact lengths are used in calculations. The details of the measurements can be found in the next section. Since the measured contact length, ℓ_{ce}', is a projection, actual contact length has to be calculated. The geometrical parameters in Fig. 2b can be calculated as follows:

$$p_1 = 2r\cos\left(\frac{\pi}{4} + \frac{\gamma+\theta_s}{2}\right)\cos\left(\frac{\gamma+\theta_s}{2}\right) \tag{3}$$

$$p_2 = 2r\sin\left(\frac{\theta_s}{2}\right)\cos\left(\gamma + \frac{\theta_s}{2}\right) \tag{4}$$

$$p_3 = 2r\sin\left(\frac{\gamma}{2}\right)\cos\left(\frac{\gamma}{2}\right) \tag{5}$$

$$\ell_6 = \ell_{ce}\,' - (p_1 + p_2 + p_3) \tag{6}$$

Sticking contact length $\ell_{pe}$is obtained by equating equation (2) to the length ℓ_{pe}:

$$l_{pe} = -l_{ce}\left(\left(\frac{\tau_1}{\mu P_0}\right)^{\frac{1}{\zeta}} - 1\right) \tag{7}$$

Forces acting on region 4

Region 4 is the first region after stagnation point, where the material is plastically deformed before

entering the flank contact region. The angle sweeping through this region is represented by θ4 (Fig. 4) since contact is an arc, and calculated as follows:

$$\theta_4 = \frac{\chi}{r} \tag{8}$$

where, r is the hone radius. If the contact length is shorter than the projected length of the 4th region then the normal forces can be calculated as follows:

$$F_{N4x} = \int_0^{ul_1} wP(\chi)\sin\frac{\chi}{r}d\chi$$

$$F_{N4y} = \int_0^{ul_1} wP(\chi)\cos\frac{\chi}{r}d\chi \tag{9}$$

where, w is the depth of cut,ul_1 is the upper limit calculated using equation (11), by solving equation (10) for θ.

$$l_{ce}{}' - p_1 = r\cos(\gamma+\theta_s)\sin\theta + r\sin(\gamma+\theta_s)\cos\theta - r\sin(\gamma+\theta_s) \tag{10}$$

$$ul_1 = r\theta \tag{11}$$

There may be three conditions for the frictional forces: only sliding, only sticking, and both sliding and sticking contact. If the contact condition in region 4 is only sliding, frictional forces are calculated as follows:

$$F_{F4x} = \int_0^{ul_1} \mu\, wP(\chi)\sin\frac{\chi}{r}d\chi$$

$$F_{F4y} = \int_0^{ul_1} \mu wP(\chi)\cos\frac{\chi}{r}d\chi \tag{12}$$

If the contact condition in region 4 is only sticking then friction forces are given as:

$$F_{F4x} = \int_0^{ul_1} \tau_1 w\cos\frac{\chi}{r}d\chi$$

$$F_{F4y} = \int_0^{ul_1} \tau_1 w\sin\frac{\chi}{r}d\chi \tag{13}$$

If contact conditions involve both sticking and sliding, then the frictional forces become:

$$F_{F4x} = \int_0^{l_{pe}} \tau_1 w\cos\frac{\chi}{r}d\chi + \int_{l_{pe}}^{ul_1} \mu wP(\chi)\sin\frac{\chi}{r}d\chi$$

$$F_{F4y} = \int_0^{l_{pe}} \tau_1 w\sin\frac{\chi}{r}d\chi + \int_{l_{pe}}^{ul_1} \mu wP(\chi)\cos\frac{\chi}{r}d\chi \tag{14}$$

Orientation of forces for all regions is shown in Fig. 4.

If the contact length is longer than the fourth region, ul_1 can be calculated as follows:

$$ul_1 = r\theta_s \tag{15}$$

Forces acting on region 5

Region 5 is responsible for the beginning of flank contact which is a result of the elastic recovery of the material deformed in front of region 4. Angle sweeping through this region (Fig. 4) is defined by θ_5 which can be calculated as:

$$\theta_5 = \frac{\chi}{r} \tag{16}$$

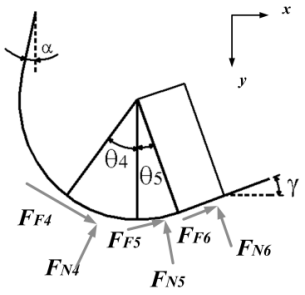

Fig. 4: Force orientations.

Contact conditions in region 5 vary as in the 4th region, and forces are calculated as the same way except the lower limit of the integral is taken as the length of region 4 (equation (15)) and upper limit is taken as ul_2.

For instance, if the contact length is shorter than the length of region 5, then the normal forces can be calculated as follows:

$$F_{N5x} = \int_{ul1}^{ul_2} wP(\chi)\sin\frac{\chi}{r}d\chi$$

$$F_{N5y} = \int_{ul1}^{ul_2} wP(\chi)\cos\frac{\chi}{r}d\chi \tag{17}$$

where, ul_2 can be calculated using equation (19), by solving equation (18) for theta.

$$l_{ce}{}' - p_1 - p_2 = r\cos(\gamma)\sin\theta - r\sin(\gamma)\cos\theta + r\sin(\gamma) \tag{18}$$

$$ul_1 = r\theta \tag{19}$$

The same equations are applied to the calculation of the frictional forces. If the total contact length is longer than the length of region 5 then ul_1 and$ul_2$are calculated as follows:

$$ul_2 = r\theta$$

$$ul_1 = r\theta_5 \tag{20}$$

Forces acting on region 6

Region 6 is also responsible for the flank contact. This contact region forms a line. Normal force components can be calculated as follows:

$$F_{N6} = \int_{l_4+l_5}^{ul_3} wP(\chi)d\chi \tag{21}$$

where, ul_3 is the upper limit and can be calculated as follows:

$$ul_3 = \ell_{ce}{}' - (p_1 + p_2 + p_3) \tag{22}$$

If the contact conditions in region 6 involve only sliding, the friction forces can be calculated as follows:

$$F_{F6} = \int_{l_4+l_5}^{ul_3} \mu wP(\chi)d\chi \tag{23}$$

If the contact conditions in region 6 involve only sticking, then the frictional forces become:

$$F_{F6} = \int_{l_4+l_5}^{ul_3} \tau_1 w d\chi \tag{24}$$

If contact conditions involve both sticking and sliding, friction forces are given as:

$$F_{F6} = \int_{l_4+l_5}^{l_{pe}} \tau_1 w d\chi + \int_{l_{pe}}^{ul_3} \mu w P(\chi) d\chi \quad (25)$$

Contact line makes an angle γ with the *x* axis; so the force components are multiplied by *cosine* or *sine* according to the orientation.

3. Working of the Model

In this section solution procedure for the proposed model is presented. Shear stress $\boldsymbol{\tau}_1$ and normal stress P_0 are obtained from the analysis of the primary and secondary shear zones [27]. Friction model is also taken from [27]. Shear angle is obtained by minimum energy approach and stagnation point is taken equal to shear angle. Projected contact length l_{ce}' is obtained from experiments for different hone radii, feed and speed. With the measured data an empirical model is developed using regression analysis for l_{ce}' as follows:

$$l_{ce}' = -0.459V_c + 0.4356r + 121.01f + 150.6 \quad (26)$$

where, l_{ce}' is the total projected contact length of the third deformation zone in μm, V_c is the cutting speed (m/min), r is hone radius (μm) and f is the feed rate (mm/rev). Afterwards actual l_{ce} is obtained by finding corresponding angle, θ, from the equations (10) and (18), yielding:

$$l_{ce} = \theta r \quad (27)$$

Then, sticking contact length ℓ_{pe} is calculated by using the equation (7). With the knowledge of ℓ_{pe} friction conditions are known and the cutting forces can be calculated for each region. Upper limits for integrals can be calculated by equations (15, 19, and 20). For region 4 normal forces are obtained by equation (9). Friction forces are calculated by equation (10) if the contact conditions on the hone contact involve only sliding and (11) if only sticking. If the contact conditions involve both sticking and sliding then equation (12) is used to calculate friction forces. For region 5 forces are calculated similarly using equations (10-12) and (17). Integral limits are changed for region 5 accordingly. For region 6 normal forces are obtained by (21) where the upper limit of the integral is calculated by equation (22). Friction forces are calculated by equations (23-25) with the contact conditions of only sliding, only sticking, or both sticking and sliding respectively. Finally tangential and feed edge forces are obtained as follows:

$$F_{ex} = F_{Njx} + F_{Fjx}$$

$$F_{ey} = F_{Njy} + F_{Fjy} \quad \text{where } j=4,5,6 \quad (28)$$

4. Comparison of Predictions with the Experimental Results

In order to verify the proposed model orthogonal tube cutting tests are conducted. AISI 1050 steel is selected as the workpiece material where TPGN type 610 grade uncoated carbide tools are used. The tangential and feed forces are measured by a dynamometer. Test setup can be seen in Fig. 5(a). Triangular tools having 5^O rake angle with different hone radii (12 μm, 30 μm, and 60 μm) are used. Depth of cut is selected as 2 mm, where the cutting speed is selected as 30, 60, 100 and 250 m/min where the feed rates are 0.05, 0.1, 0.15 and 0.2 mm/rev.

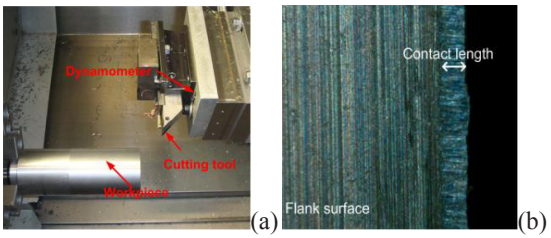

Fig. 5: (a) Test setup (b) Contact length on the flank face.

Contact lengths on the flank surface are measured by a stereomicroscope with 100x magnification, Fig. 5(b). The results showed that the developed empirical model estimated the contact length with a discrepancy of 20%.

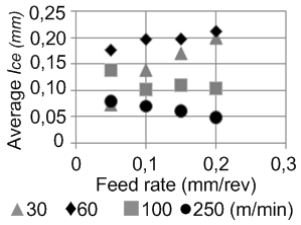

Fig. 6: Variation of the average contact length with feed and cutting speed.

Fig. 6 shows change of the average measured contact length with feed and speed. It is observed that with increased feed the contact length increases at low speeds and decreases at high speeds. Also, it can be said that there is a critical speed at which the behaviour changes; for instance at a certain feed rate increasing speed increases the contact length at low speeds, but for higher speeds it is vice versa. Also feed is more effective on the contact length at low speeds.

The experimental results along with the simulations for total forces can be seen in Fig. 7, 8 and 9. Johnson-Cook model (equation 29) and the friction model (30) used in the simulations for AISI 1050 Steel can be seen below:

$$\tau = \frac{1}{\sqrt{3}}\left[880 \times 10^6 + 500.8 \times 10^6 \left(\frac{\Upsilon}{\sqrt{3}}\right)^{0.234}\right]\left[1 + \ln\left(\frac{\dot{\Upsilon}}{0.001}\right)^{0.0134}\right]\left[1 - \frac{T-300}{1433}\right] \quad (29)$$

where Υ is the shear strain T is the absolute temperature which are calculated iteratively.

$$\mu = 6.12 \times 10^{-4} V_c + 0.398 \quad (30)$$

where V_c is cutting speed in (m/min).

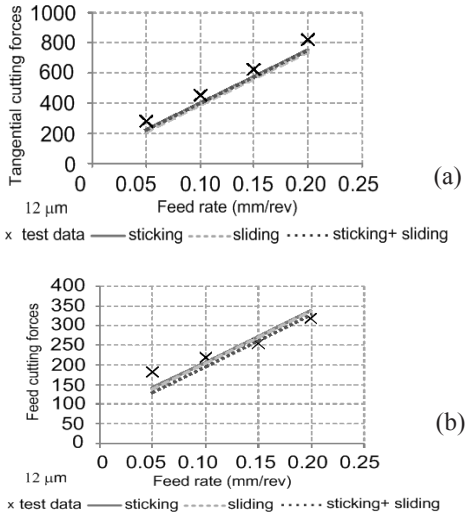

Fig. 7: Comparison of the cutting models for tool having 12 μm hone radius for (a) tangential, (b) feed cutting forces.

Both experimental and simulation results show that total forces increase with the hone radius. (Fig. 7-8) The results indicate that all of the implemented models provide comparable results with a difference of 3% for the tool with 12 μm hone radius, and 1% for the tool with 30 μm hone radius.

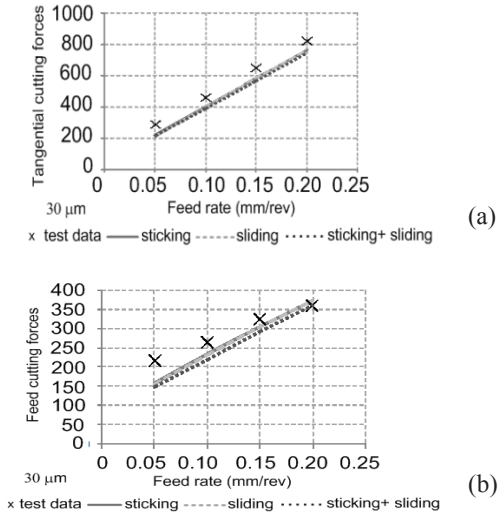

Fig. 8: Comparison of the cutting model predictions with measurements for the tool with 30 μm hone radius for (a) tangential, (b) feed cutting forces.

For the tangential forces, the discrepancy on estimation of the sliding model decreases with the increased hone radius. For sharp cutting edge the discrepancy is about 10% while it is 5% for the 30 μm honed tool. For the feed forces, on the other hand, the discrepancy can increase up to 20% when the hone radius is decreased. However, the trend is the same and the difference can be attributed to smaller force values. Inaccuracies in the contact length measurements may also have caused the difference. It was also observed that at higher feed rates simulations provide relatively better results.

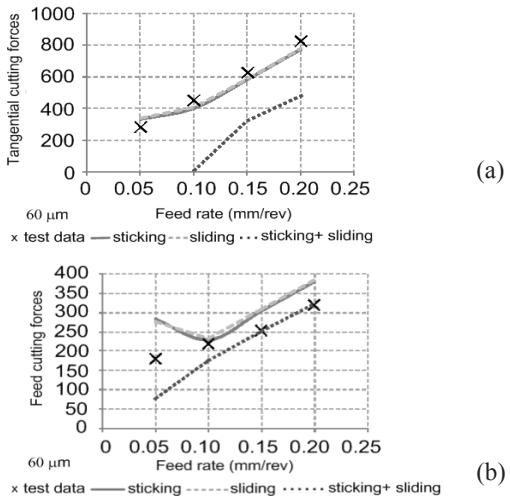

Fig. 9: Comparison of the cutting model predictions for the tool with 60 μm hone radius for (a) tangential, (b) feed cutting forces

The tangential forces obtained from the models involving only sticking and only sliding conditions are in good agreement with the tangential forces for the tool with 60 μm hone (Fig. 9), however, the discrepancy of the model with both sticking and sliding conditions increases up to 100% at lower feeds which may be a result of the discrepancy in contact length calculations. On the contrary, this model gives the best results for the feed forces. It can be said that models cannot predict forces for large hone radius at low feed rates.

Comparison of the edge forces obtained by extracting the primary and secondary zone forces from the total forces-and the proposed model can be seen in Fig. 10.

As it can be seen from the figures the tangential edge forces are estimated better than the feed edge forces. All of the analytical models provide similar trends and comparable results. The discrepancy is found to be around 40% for the tangential edge forces and 50% for the feed edge forces of 12 μm honed tool. One major reason for the discrepancy is relatively higher measurement uncertainty due to very small forces. When experimental data is considered, it is observed from the graphs that the tangential edge forces lie on a line and do not vary with the feed as in the linear edge force model. However, the feed edge forces vary with the feed which is the result of calculated primary and secondary shear zone forces.

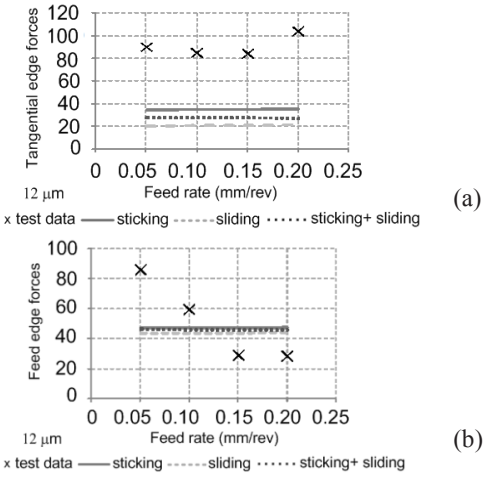

Fig. 10: Tangential edge forces (a) and feed edge forces (b) for 12μm hone radius. "x" markers represent the edge forces obtained by extracting calculated cutting forces (except edge forces) from measured total forces and the lines represent the simulation results.

5. Conclusions

In this study a process model including the effect of hone radius and flank contact on cutting forces is presented. The proposed model is verified with orthogonal tube cutting tests conducted on AISI 1050 steel. The following are the main observations from analytical and experimental results.

- The total contact length increases with the feed at low cutting speeds and decreases at high speeds. Increasing cutting speed at low feed rates increases the contact length whereas at high feed rates it has the opposite effect. This behavior could be explained by changes in the workpiece temperature at the hone edge for higher feed rates. Increased temperature due to higher speed reduces the yield strength, and thus the elastic deformation and recovery, resulting in shorter contact length. For low feed rates, on the other hand, the contact is influenced more by the friction conditions.
- Total cutting forces increase with the hone radius as shown by both analytical and experimental results.
- Implemented model predictions are in a good agreement with the measurements as the discrepancy is about 3%.
- Tangential forces are estimated more accurately compared to the feed forces. High discrepancy on feed forces can be related to smaller force values since force trends are in a good agreement for both tangential and feed forces.
- For 60 μm hone radius, models based on only sticking and only sliding contact are in good agreement with the measured tangential forces. On the other hand, model involving both sticking and sliding conditions provide better results for the feed forces. At low feed rates, all models have high discrepancies which may be the result of contact length predictions. Smaller forces at low feeds, and thus poor signal-to-noise ratio also contribute to this.
- Feed edge forces obtained from experimental data strongly depend on feed rate. It can be said that tangential edge forces are predicted better than feed edge forces in terms of force trends. The discrepancy between edge forces obtained from experimental data and model is found to be 40% for tangential edge forces whereas it is 50% for feed edge forces.

References

[1] Albrecht, P., 1960, New Developments in the Theory of the Metal-Cutting Process: Part I. The Ploughing Process in Metal Cutting, J. Eng. for Industry 82, pp. 348-358.
[2] Endres, J. W., Manjunathaiah, J., 2000, A New Model and Analysis of Orthogonal Machining With an Edge-Radiused Tool, Manuf. Sci. Eng. 122, 384.
[3] Kountanya, R.K. , Endres, W.J., 2001, A High-Magnification Experimental Study of Orthogonal Cutting with Edge-honed Tools, ASME MED, v12, pp. 157–163.
[4] Fang, N., 2003, Slip-line Modeling of Machining with a Rounded-edge tool—Part I: New Model and Theory, Journal of the Mechanics and Physics of Solids, Volume 51, Issue 4, pp. 715-742.
[5] Waldorf, D. J., 2006, A Simplified Model for Ploughing Forces in Turning, J. of Manuf. Processes, Volume 8, Issue 2, pp. 76-82.
[6] Endres, W.J., Kountanya, R.K., 2002, The Effects of Corner Radius and Edge Radius on Tool Flank Wear,Transactions of NAMRI/SME, v30, pp. 401–407.
[7] Özel, T., 2003, Modelling of Hard Part Machining: Effect of Insert Edge Preparation in CBN Cutting Tools, Journal of Materials Processing Technology, 141, pp. 284–293.
[8] Özel T., Hsu T-K., Zeren E., 2005, Effects of Cutting Edge Geometry, Workpiece Hardness, Feed Rate and Cutting Speed on Surface Roughness and Forces in Finish Turning of Hardened AISI H13 steel. Int J AdvManufTechnol 25:262-269.
[9] Ranganath, S., Campbell, A. B., Gorkiewicz, D. W., 2007, A Model to Calibrate and Predict Forces in Machining with Honed cutting Tools or Inserts, International Journal of Machine Tools and Manufacture, Volume 47, Issue 5, pp. 820-840.
[10] Wyen, C.-F., Wegener, K., 2010, Influence of Cutting Edge Radius on Cutting Forces in Machining Titanium, CIRP Annals - Manufacturing Technology, Volume 59, Issue 1, pp. 93-96.
[11] Bassett, E., Köhler, J., Denkena, B., 2012, On The Honed Cutting Edge and its Side Effects During Orthogonal Turning Operations of AISI1045 with Coated WC-Co Inserts, CIRP J. of Manuf. Sci. and Tech., Volume 5, Issue 2, pp. 108-126.
[12] Yen, Y.-Ch., Jain, A., Altan, T., 2004, A Finite Element Analysis of Orthogonal Machining Using Different Tool Edge Geometries, J. Mater.Proc.Technol., Vol. 146, pp. 72-81.
[13] Fang, N., Fang, G., 2007, Theoretical and experimental investigations of finish machining with a rounded edge tool, J. of Mat. Proc. Technology, Volume 191, Issues 1–3, pp. 331-334.
[14] ÖZEL T., 2009, Computational Modelling of 3D Turning: Influence of Edge Micro-geometry on Forces, Stresses, Friction and Tool Wear in PcBN Tooling, Journal of Materials Processing Tech. vol. 209/11, pp. 5167-5177.
[15] Özel, T., Karpat, Y., Srivastava, A.K., 2008, Hard turning with variable micro-geometry PcBN tools. CIRP Annals—Manufacturing Technology 57, pp. 73–76.
[16] Dudzinski, D., and Molinari, A., 1997, A Modeling of Cutting for Viscoplastic Materials, Int. J. Mech. Sci, 39/4:369-389
[17] Özlü, E., Molinari, A.,Budak, E., 2010, Two-zone Analytical Contact Model Applied to Orthogonal Cutting.Machining Science and Technology, 14 (3). pp. 323-343.